Inorganic Chemistry

pubs.acs.org/IC Article

Nature of the Short Rh−Li Contact between Lithium and the Rhodium ω-Alkenyl Complex $[Rh(CH_2CMe_2CH_2CH{=}CH_2)_2]^-$

Sumeng Liu, Brett A. Smith, Justin K. Kirkland, Konstantinos D. Vogiatzis,* and Gregory S. Girolami*

Cite This: *Inorg. Chem.* 2021, 60, 8790−8801 Read Online

ACCESS | Metrics & More | Article Recommendations | Supporting Information

ABSTRACT: We describe the preparation of the *cis*-bis(η^1,η^2-2,2-dimethylpent-4-en-1-yl)rhodate(I) anion, *cis*-$[Rh(CH_2CMe_2CH_2CH{=}CH_2)_2]^-$, and the interaction of this species with Li^+ both in solution and in the solid state. For the lithium(diethyl ether) salt $[Li(Et_2O)][Rh(CH_2CMe_2CH_2CH{=}CH_2)_2]$, VT-NMR and $^1H\{^7Li\}$ NOE NMR studies in toluene-d_8 show that the Li^+ cation is in close proximity to the d_{z^2} orbital of rhodium. In the solid-state structure of the lithium(12-crown-4) salt $[Li(12\text{-crown-}4)_2][Li\{Rh(CH_2CMe_2CH_2CH{=}CH_2)_2\}_2]$, one lithium atom is surrounded by two $[Rh(CH_2CMe_2CH_2CH{=}CH_2)_2]^-$ anions, and in this assembly there are two unusually short Rh−Li distances of 2.48 Å. DFT calculations, natural energy decomposition, and ETS-NOCV analysis suggest that there is a weak dative interaction between the $4d_{z^2}$ orbitals on the Rh centers and the $2p_z$ orbital of the Li^+ cation. The charge-transfer term between Rh and Li^+ contributes only about the 1/5 of the total interaction energy, however, and the principal driving force for the proximity of Rh and Li in compounds **1** and **2** is that Li^+ is electrostatically attracted to negative charges on the dialkylrhodiate anions.

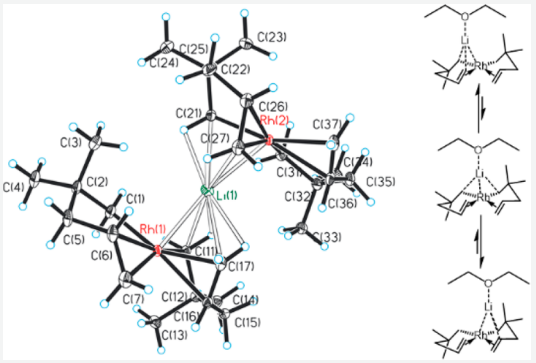

INTRODUCTION

The chemistry of complexes with metal−metal bonds has seen a strong resurgence of interest in recent years.[1] Especially interesting are compounds in which the metal−metal bonds involve two metals of different electronegativity: such compounds are able to activate small molecules such as H_2 and N_2.[2−10] As the electronegativity difference between the metals increases, the bonding necessarily becomes less covalent. Compounds that combine very electropositive metals, such as Li and Mg, with very electronegative metals, such as electron-rich late transition metals, show potential as catalysts for organic reactions such as cross-coupling[11−14] and cycloaddition reactions.[15,16] Understanding the interactions between these metal centers is important for the development of the chemistry of these complexes.[12]

Several dozen compounds are known that exhibit relatively short M−M distances between a group 8 transition metal and a Li[11−14,16−37] or a Mg[38−53] center. In some of these compounds, the two metal centers are best described as noninteracting and are held in close proximity by electron-rich anionic ligands.[22,40,50] In other compounds, the M−M interaction has been described in a variety of ways: ion pairing,[23,27,30] dative bonding (coordinate bonding),[54] p−d π bonding,[55] and three-center bonding mediated by an anionic ligand.[32,56,57] In a few cases, covalent interactions have been suggested.[12,44] Despite this variety in the description of the M−M interaction, modern computational studies generally suggest that the interactions between Li or Mg and late transition metals are predominantly ionic and that covalent (dative) interactions play a minor role at best.[37,43,52,53,58]

Rhodium forms a variety of heterobimetallic complexes with main-group metals,[59−61] transition metals,[62] and f-block elements.[63] Of these, one complex is known, [Li(TMEDA)][(COD)Rh(CH_2SiMe_3)$_2$],[31] in which the Li−Rh distance is shorter than the 2.70 Å sum of the covalent radii of lithium (1.28 Å) and rhodium (1.42 Å).[64] This Li−Rh interaction was judged to be the result of ion pairing[23] in which the Li^+ cation is attracted to the negative charges around the Rh center[65] rather than Rh to Li dative bonding.[54] Thus, despite the presence of a short contact, the Li−Rh orbital overlap in [Li(TMEDA)][(COD)Rh(CH_2SiMe_3)$_2$] was proposed to be small.[31] Some other lithium salts of anionic rhodium(I) alkyls and aryls are known, but these compounds were not crystallographically characterized.[66]

We have recently described the synthesis of several platinum(II) complexes in which two ω-alkenyl ligands chelate to the metal center by means of a σ-bond at one end of the alkenyl chain and a π-bond at the other.[67] We now report the synthesis and characterization of two related rhodium

Received: March 10, 2021
Published: June 7, 2021

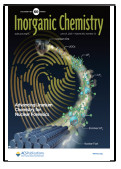

https://doi.org/10.1021/acs.inorgchem.1c00737
Inorg. Chem. 2021, 60, 8790−8801

compounds containing the *cis*-[Rh($CH_2CMe_2CH_2CH{=}CH_2$)$_2$]$^-$ anion. One of the two compounds, which has been characterized crystallographically, contains the shortest Li−Rh contact seen in any compound. The nature of the Li−Rh interactions in this molecule has been probed both by solution NMR and by DFT calculations, and the results of this investigation indicate that the interactions are predominantly ionic despite the short contact distance.

RESULTS AND DISCUSSION

Synthesis and Crystal Structure of the *cis*-[Rh($CH_2CMe_2CH_2CH{=}CH_2$)$_2$]$^-$ Anion. Treatment of rhodium(I) ethylene complex $Rh_2Cl_2(CH_2{=}CH_2)_4$ with 4 equiv of (2,2-dimethylpent-4-en-1-yl)lithium[68] in pentane/diethyl ether results in conversion to the air- and heat-sensitive organorhodate salt [Li(Et_2O)][Rh($CH_2CMe_2CH_2CH{=}CH_2$)$_2$] (**1**). By carrying out the same reaction except with the addition of 12-crown-4, we succeeded in obtaining X-ray-quality crystals of the related salt [Li(12-crown-4)$_2$][Li{Rh($CH_2CMe_2CH_2CH{=}CH_2$)$_2$}$_2$] (**2**). Compound **1** decomposes within hours under argon at room temperature, making its isolation difficult. Solid samples of **2** are indefinitely stable under argon at −20 °C but decompose when dissolved in toluene at room temperature. Crystal data for the [Li(12-crown-4)$_2$]$^+$ salt **2** are listed in Table 1, and selected bond lengths and angles are collected in Table 2. The crystal structure shows that **2** is an ionic solid with charge-separated [Li{Rh($CH_2CMe_2CH_2CH{=}CH_2$)$_2$}$_2$]$^-$ anions (Figure 1) and [Li(12-crown-4)$_2$]$^+$ cations (Figure 2). The structure of the [Rh($CH_2CMe_2CH_2CH{=}CH_2$)$_2$]$^-$ unit is similar to that of the Pt analog Pt($CH_2CMe_2CH_2CH{=}CH_2$)$_2$ (**3**):[67] both pentenyl ligands chelate to the metal center by means of a σ bond at one end of the pentenyl chain and a π bond at the other. The Rh-bound pentenyl ligands both adopt chair conformations in which the two Rh−C σ-bonds are cis to one another (as are the two π bonds).

Interestingly, one of the lithium cations in **2** is sandwiched between two square-planar [Rh($CH_2CMe_2CH_2CH{=}CH_2$)$_2$]$^-$ units; the latter are arranged with nearly ideal (but non-crystallographic) inversion symmetry about the Li center. The Li$^+$ cation forms short contacts with both of the [Rh($CH_2CMe_2CH_2CH{=}CH_2$)$_2$]$^-$ units: the shortest Li−C contacts involve one of the two α-carbon atoms in each Rh unit (Li−C = 2.410 (4) Å and 2.448 (4) Å) and the terminal olefinic carbon on the same ligand (Li−C = 2.711 (4) Å and 2.602 (4) Å). Interestingly, the Rh−C_δ and Rh−C_ε bonds of 2.20 and 2.15 Å, respectively, to the olefin that interacts with Li are shorter than the corresponding Rh−C bonds of 2.23 and 2.20 Å to the noninteracting olefin. Consistent with the shorter Rh−olefin distance, the C=C distance, 1.396 Å, in the olefin that interacts with Li is longer than the C=C distance of 1.375 Å in the noninteracting olefin. We conclude that interaction of the lithium center with the olefin makes the latter a better

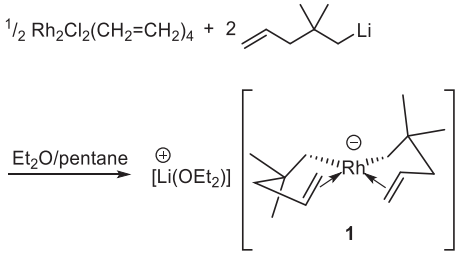

Table 1. Crystallographic Data for [Li(12-crown-4)$_2$][Li{Rh($CH_2CMe_2CH_2CH{=}CH_2$)$_2$}$_2$] (2)

space group, $P2_1/c$	formula, $C_{44}H_{84}Li_2O_8Rh_2$
T = 100 K	FW = 960.81 g/mol
λ = 0.71073 Å	V = 4720.0(2) Å^3
a = 12.5784(4) Å	Z = 4
b = 14.8411(4) Å	ρ_{calc} = 1.352 g/cm^3
c = 25.3705(7) Å	μ = 0.75 mm^{-1}
β = 94.7303(6)°	R(int) = 0.034
absorption correction: face indexed	
max., min transm. factors: 0.9695, 0.9142	
data, restraints, params: 10418, 16, 683	
GOF on F^2: 1.146	
R_1 [$I > 2\sigma(I)$][a] = 0.0259; wR_2 (all data)[b] = 0.0516	
max, min $\Delta\rho_{electron}$, 0.64, −0.48 e/Å^3	

[a] $R_1 = \Sigma\,||F_0| - |F_c||/\Sigma|F_0|$. [b] $wR_2 = [\Sigma w(F_0^2 - F_c^2)^2/\Sigma(F_0^2)^2]^{1/2}$.

acceptor, thus increasing the amount of π-backbonding from rhodium.

The interaction between the C=C bonds and Li$^+$ affects not only the C=C bond distances but also the conformations of the pentenyl ligands. We previously showed that, in the Pt analog **3**, the angle between the C=C bond vectors and the normal to the square plane, which we called the tilt angle, averaged 29°. Usually in d^8 square-planar olefin complexes, the olefin is perpendicular to the square plane (tilt angle of 0°); we attributed the tilted conformation in **3** to the shortness of the pentenyl chain, steric hindrance, and crystal packing effects.[67] In contrast, for the Rh complex **2**, the average tilt angle of the noninteracting olefins is 50°, whereas the average tilt angle of the interacting olefins is 17° (i.e., more nearly perpendicular to the square plane). Similarly, the Rh−C_α−C_β bond angle also decreases from 117.5(2)° for the noninteracting ligand to 105.0(2)° for the interacting ligand. The changes in bond angles and tilt angles must be due to the interaction of the α-C and the terminal olefinic carbon with the Li$^+$ cation.

Hydrogen atoms were included in calculated positions in the crystallographic model; these calculated positions suggest that there are four short Li−H contacts, one on each of the four carbon atoms involved in short Li−C distances: two of these are to α-C−H atoms, one on each of the two pentenyl ligands, Li−H = 2.02 (2) and 2.08 (2) Å, and two somewhat longer contacts are to δ-C−H atoms, again on each of the pentenyl ligands, Li−H = 2.33 (2) and 2.21(2) Å.

In addition to the Li−C and Li−H contacts in **2**, there are also two short Li−Rh contacts of 2.470(3) Å to one [Rh($CH_2CMe_2CH_2CH{=}CH_2$)$_2$]$^-$ unit and 2.482(3) Å to the other; the Rh−Li−Rh angle of 156.60 (16)° is close to linear. These Li−Rh distances are shorter than that of 2.563(9) Å seen previously in the alkylrhodate salt [Li(TMEDA)][(COD)Rh(CH_2SiMe_3)$_2$].[31]

Notably, all of these Li−Rh distances are considerably shorter than the 2.70 Å sum of the covalent radii of lithium (1.28 Å) and rhodium (1.42 Å).[64] The Li$^+$ cation is located very close to one of the two vacant axial positions in the square-planar coordination environment about each Rh ion, which raises the question whether there is an interaction between lithium and the filled d_{z^2} orbitals on rhodium. We will return to this point below.

NMR Studies of the [Rh($CH_2CMe_2CH_2CH{=}CH_2$)$_2$]$^-$ Anion. The ^{1}H and ^{13}C NMR spectra of the lithium-diethyl ether salt **1** (Figures 3 and 4) are very similar to those reported

https://doi.org/10.1021/acs.inorgchem.1c00737
Inorg. Chem. 2021, 60, 8790−8801

Table 2. Selected Bond Distances and Angles for $[Li(12\text{-crown-4})_2][Li\{Rh(CH_2CMe_2CH_2CH{=}CH_2)_2\}_2]$ (2)

bond distances (Å)			
Li1—Rh1	2.482 (3)	Li1—Rh2	2.470 (3)
Li1—C11	2.410 (4)	Li1—C21	2.448 (4)
Li1—C17	2.711 (4)	Li1—C27	2.602 (4)
Li1—H11A	2.02 (2)	Li1—H21A	2.08 (2)
Li1—H17A	2.33 (2)	Li1—H27A	2.21 (2)
Rh1—C1	2.105 (2)	Rh2—C21	2.110 (2)
Rh1—C11	2.111 (2)	Rh2—C31	2.098 (2)
Rh1—C6	2.227 (2)	Rh2—C26	2.195 (2)
Rh1—C16	2.208 (2)	Rh2—C36	2.235 (2)
Rh1—C7	2.189 (2)	Rh2—C27	2.151 (2)
Rh1—C17	2.157 (2)	Rh2—C37	2.204 (2)
C1—C2	1.539 (3)	C11—C12	1.543 (3)
C2—C3	1.525 (3)	C12—C13	1.542 (3)
C2—C4	1.537 (3)	C12—C14	1.533 (3)
C2—C5	1.533 (3)	C12—C15	1.540 (3)
C5—C6	1.512 (3)	C15—C16	1.514 (3)
C6—C7	1.376 (3)	C16—C17	1.393 (3)
C21—C22	1.538 (3)	C31—C32	1.540 (3)
C22—C23	1.536 (3)	C32—C33	1.532 (3)
C22—C24	1.539 (3)	C32—C34	1.534 (3)
C22—C25	1.540 (3)	C32—C35	1.528 (3)
C25—C26	1.523 (3)	C35—C36	1.511 (3)
C26—C27	1.398 (3)	C36—C37	1.374 (3)
bond angles (deg)			
Rh1—Li1—Rh2	156.60 (16)		
C11—Li1—C21	132.13 (16)	C17—Li1—C27	82.52 (12)
C11—Li1—C17	72.52 (11)	C21—Li1—C27	72.85 (11)
C11—Li1—C27	155.01 (17)	C21—Li1—C17	155.17 (16)
C1—Rh1—C7	105.80 (8)	C21—Rh2—C27	89.54 (8)
C1—Rh1—C11	85.90 (7)	C21—Rh2—C31	85.98 (8)
C1—Rh1—C17	154.38 (8)	C21—Rh2—C37	159.85 (8)
C7—Rh1—C11	157.73 (8)	C27—Rh2—C31	157.28 (8)
C7—Rh1—C17	86.41 (8)	C27—Rh2—C37	86.27 (8)
C11—Rh1—C17	90.77(7)	C31—Rh2—C37	105.09 (8)
Rh1—C11—Li1	66.20 (10)	Rh2—C21—Li1	65.13 (9)
Rh1—C17—Li1	60.02 (9)	Rh2—C27—Li1	61.76 (9)
C2—C1—Rh1	117.36 (13)	C12—C11—Rh1	105.05 (11)
C22—C21—Rh2	104.96 (12)	C32—C31—Rh2	117.68 (14)
C5—C2—C1	104.77 (15)	C15—C12—C11	106.34 (15)
C21—C22—C25	106.79 (16)	C35—C32—C31	105.48 (16)
C6—C5—C2	110.31 (15)	C16—C15—C12	111.53 (15)
C26—C25—C22	111.50 (16)	C36—C35—C32	111.77 (16)
C5—C6—C7	123.3 (2)	C15—C16—C17	121.52 (17)
C25—C26—C27	121.27 (19)	C35—C36—C37	122.33 (19)

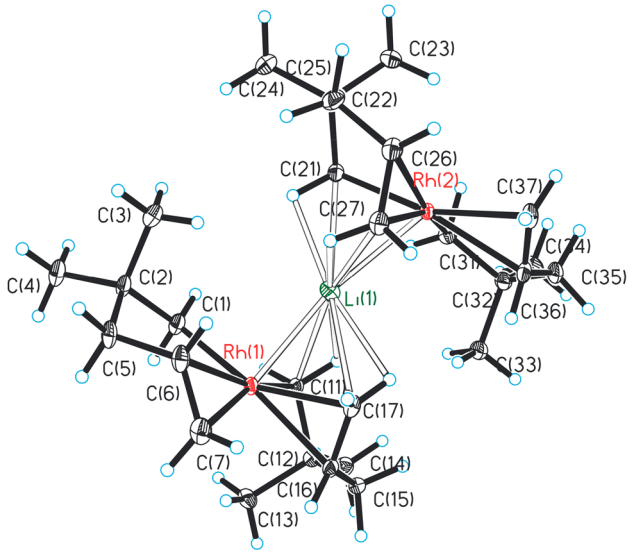

Figure 1. Molecular structure of the $[Li\{Rh(CH_2CMe_2CH_2CH{=}CH_2)_2\}_2]^-$ anion in **2**. Ellipsoids are drawn at the 35% probability level.

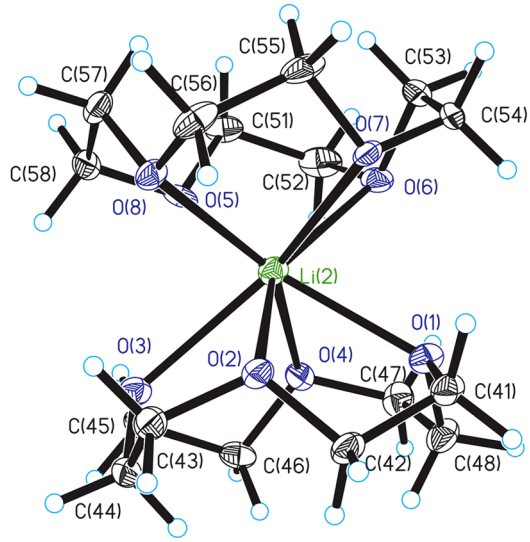

Figure 2. Molecular structure of the $[Li(12\text{-crown-4})_2]^+$ cation in **2**. Ellipsoids are drawn at the 35% probability level. Only the major conformer is shown for clarity.

for the platinum analog $Pt[CH_2CMe_2CH_2CH{=}CH_2]_2$ (**3**).[67] Several lines of evidence show that, in toluene at room temperature, the two 2,2-dimethylpent-4-en-1-yl ligands in **1** coordinate to rhodium in the same η^1, η^2 fashion as seen in the Pt analog **3**:[67] (1) for the olefinic protons, the ^{1}H NMR chemical shifts are shielded and the $^3J_{HH}$ coupling constants are smaller relative to those seen for uncoordinated olefins[69−72] and for olefins coordinated to lithium;[68] (2) the CMe_2 groups are diastereotopic, as are the α- and γ-CH_2 protons within the 2,2-dimethylpent-4-en-1-yl ligands; this symmetry breaking, which is expected if the pentenyl ligands are chelating to rhodium, shows that decomplexation of the Rh−olefin interaction is slow at room temperature, as it is for the Pt analog **3**;[67] (3) all of the ^{1}H−^{1}H coupling constants are almost identical to those in the Pt analog **3**. The Pt complex **3** undergoes an olefin decomplexation process that exchanges the distereotopic groups; this process is slow on the NMR time scale at room temperature and below but becomes fast at higher temperatures. For the Rh compound **1**, there is no evidence of this process at −50 °C (Figure S15); investigations at room temperature and above are challenging because the rate of decomposition becomes fast.

In solution, the pentenyl ligands in **1** evidently adopt chair conformations like those seen in **3**, as shown by the observation of an ∼2 Hz long-range (four-bond) coupling between one of the α-CH_2 protons and one of the γ-CH_2 protons (Figure S12). The magnitude of this coupling, which should follow a Karplus-type dependence on the dihedral angle relating the two C−H bonds,[73,74] is consistent with a H−C−

https://doi.org/10.1021/acs.inorgchem.1c00737
Inorg. Chem. 2021, 60, 8790−8801

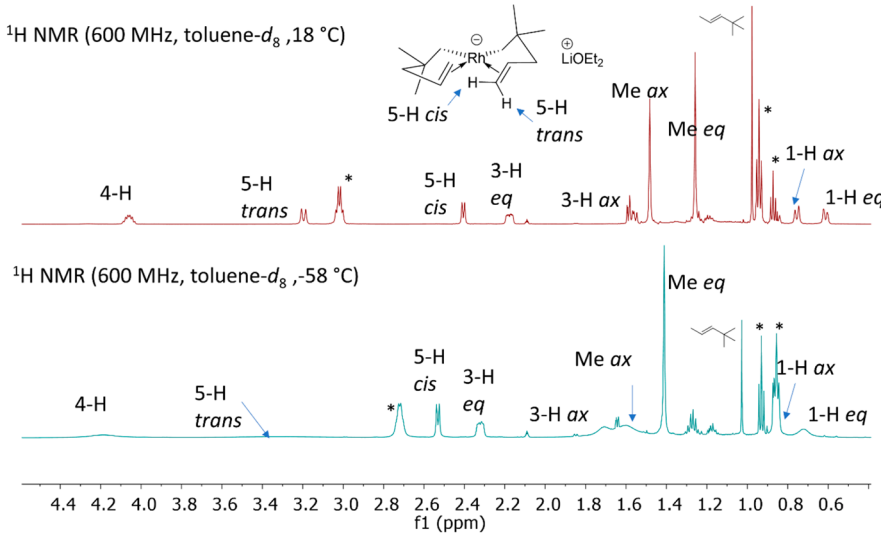

Figure 3. ^{1}H NMR spectrum of $[Li(Et_2O)][Rh(CH_2CMe_2CH_2CH{=}CH_2)_2]$ (**1**) at 18 and −58 °C in toluene-d_8. Peaks labeled with asterisks are due to coordinated diethyl ether or pentane.

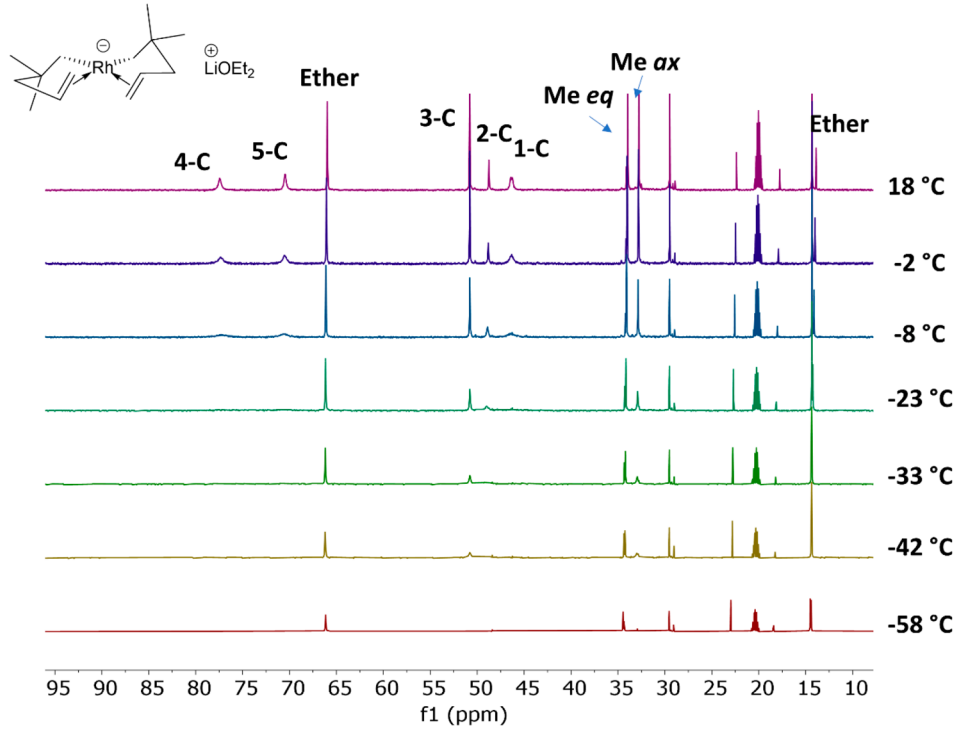

Figure 4. VT $^{13}C\{^{1}H\}$ NMR spectrum of $[Li(Et_2O)][Rh(CH_2CMe_2CH_2CH{=}CH_2)_2]$ (**1**) in toluene-d_8.

C−C−H dihedral angle involving two equatorial protons in a chair structure.

The $^{7}Li\{^{1}H\}$ spectrum of **1** in toluene at 20 °C shows a singlet at δ 0.40 characteristic of lithium cations.[75] Although $^{7}Li-^{195}Pt$ couplings have been seen in some platinum(II) acetylides,[21] in **1** there is no observable coupling between ^{7}Li (or ^{6}Li) and the ^{103}Rh nucleus, which is not surprising in view of the small gyromagnetic ratio for ^{103}Rh. The ^{1}H NMR spectrum contains peaks due to Li-coordinated diethyl ether, with chemical shifts that are shielded compared to those for free diethyl ether in toluene (δ 3.25, 1.10).[76] NMR integrations show that there is one diethyl ether molecule for every two pentenyl ligands (Figure S11). This ratio, which corresponds to one diethyl ether molecule per lithium atom, strongly suggests that, in toluene, the $[Li(Et_2O)]^{+}$ cations form contact ions with the $[Rh(CH_2CMe_2CH_2CH{=}CH_2)_2]^{-}$ anions. These contact ions must be dynamic and in the fast-exchange regime in the room-temperature NMR spectra because if exchange were slow then the two pentenyl ligands would be chemically inequivalent.

There is evidence that the exchange process involving the contact ions slows at lower temperatures. Cooling a solution of **1** in toluene-d_8 to −58 °C results in broadening of the resonances due to the $[Rh(CH_2CMe_2CH_2CH{=}CH_2)_2]^{-}$ anion (Figures 3 and 4),[31,66] although even at −58 °C the exchange process is still in the fast exchange regime.

https://doi.org/10.1021/acs.inorgchem.1c00737
Inorg. Chem. 2021, 60, 8790−8801

Interestingly, as the sample is cooled, the ^{1}H NMR resonances for the axial substituents of the chair-shaped pentenyl group broaden much more than the resonances for the equatorial substituents; in addition, the resonance for the olefinic $=CH_2$ proton that is trans to the olefinic methine proton broadens much more than the resonance for the cis olefinic $=CH_2$ proton.

We propose that the selective broadening is due to slowing of the movement of the $[Li(Et_2O)]^+$ cation from one side of the Rh square plane to the other by either a unimolecular or bimolecular mechanism; a similar process has been proposed to occur in $[Li(tmeda)_2][(Bu^t_2PCH_2CH_2PBu^t_2)Rh(p\text{-}C_6H_4Me)_2]$.[66] A static interaction with one $[Li(Et_2O)]^+$ cation would desymmetrize the pentenyl ligands in the $[Rh(CH_2CMe_2CH_2CH{=}CH_2)_2]^-$ anion: if we consider the two axial Me groups (indicated by black circles in Scheme 1), then this static interaction would make the two axial Me groups chemically inequivalent, and the same would be true for the axial protons of the CH_2 groups. Movement of the $[Li(Et_2O)]^+$ cation to the other side of the Rh square plane exchanges the proximal (site A) groups with the distal (site B) group. Even though at −58 °C exchange between these two sites is rapid enough that the line shape is still above the coalescence point (so that only a single A/B resonance is seen), it is slow enough to cause the line width of the exchange-averaged NMR resonance to be larger at −58 °C than at room temperature.

For an exchange process between two sites A and B of equal populations in the fast-exchange regime, the increase in the NMR line width at half-height due to exchange broadening is given by $^1/_2\pi\Delta\nu^2/k$, where $\Delta\nu$ is the Larmor frequency difference between sites A and B and k is the exchange rate.[77] At room temperature, at which the exchange is in the fast exchange limit, the ^{1}H NMR line widths for all of the resonances due to **1** are small and rather similar (Figure 1).

At any one temperature in the fast-exchange regime, k is a constant for all of the sites that are interchanged by the exchange process so that the extra broadening seen for each resonance depends only on $\Delta\nu$ for that pair of exchanging sites. A Li^+ cation may affect the chemical shifts of nearby nuclei by two mechanisms: first, by polarizing its neighborhood and creating a local electric field;[78] second, by sterically affecting local interactions with solvent molecules. Thus, in the frozen structure, if the proximal (A) protons are relatively close to the Li^+ cation (so that site A is chemically distinct from distal site B), then $\Delta\nu$ should be larger. In contrast, if the proximal (A) protons are relatively far from the Li^+ center (so that site A more closely resembles distal site B), then $\Delta\nu$ should be smaller. Therefore, at a given temperature, the exchange-averaged resonances that show the greatest broadening indicate which proximal protons are closest to the Li^+ center in the static structure.

Scheme 1. Desymmetrization of Pentenyl Ligands in 1 by Interaction with the Li Cation

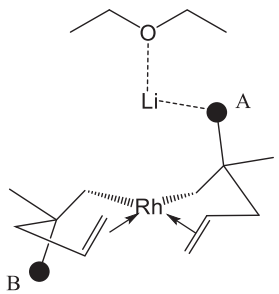

For the $[Li(Et_2O)]^+$ salt **1**, the more significant line broadening seen (Figure 3) for the axial methyl and axial CH_2 groups in the pentenyl ligand (and for the olefinic $=CH_2$ proton that is trans to the olefinic methine proton) strongly suggests that, in the frozen structure, the proximal (A) protons of these groups are closest to the Li^+ center. For example, at −2 °C, the line widths of the axial methyl (3.72 Hz) and equatorial methyl resonances (2.17 Hz) are similar, but at −42 °C, the line width of the axial methyl resonance (18.78 Hz) is significantly larger than that of its equatorial counterpart (3.26 Hz). We can estimate from the increases in line widths upon cooling that the chemical shift difference between the A and B sites is approximately 4 times larger for the axial Me groups than it is for the equatorial Me groups.

In the Pt analog **3**, the ^{1}H NMR chemical shifts of the two olefinic $=CH_2$ protons (i.e., cis and trans to the olefinic methine proton) differ by $\delta_{trans} - \delta_{cis} \approx 0.2$ ppm, whereas in **1**, $\delta_{trans} - \delta_{cis} \approx 0.8$ ppm. In **1**, the trans resonance broadens at lower temperature but the cis resonance does not. In view of the structural similarity between **1** and its Pt analog **3**, it is reasonable to attribute the larger value of $\delta_{trans} - \delta_{cis}$ seen for **1** to a $2 \times (0.8-0.2) = 1.2$ ppm deshielding of the chemical shift of the proximal trans proton vs its distal counterpart, as a result of its interaction with Li^+.[68]

Broadening of the $^{13}C\{^1H\}$ NMR resonances of **1** is also observed at low temperature (Figure 4). When a solution of **1** in toluene-d_8 is cooled from 20 °C, the resonances of the Rh-bound carbon atoms broaden more rapidly than the resonances for those not bound to rhodium. Thus, the resonances due to the α-CH_2 (Rh−C = 2.10 Å), olefinic methine (Rh−C = 2.23 Å), and olefinic methylene (Rh−C = 2.20 Å) carbon atoms broaden first and at −23 °C cannot be distinguished from the baseline; the β-C (Rh−C = 3.13 Å), γ-CH_2 (Rh−C = 3.13 Å), and axial methyl carbon resonances (Rh−C = 3.81 Å) broaden and disappear into the baseline by −58 °C. The resonance due to the equatorial methyl carbons (which are farthest from the Rh center; Rh−C = 4.44 Å) also broadens, but to a lesser extent, and it is still above the baseline at −58 °C. As we have suggested above, more significant broadening means a larger perturbation of the chemical shift of the proximal sites caused by interactions with the Li^+ cation. The more significant broadening of the ^{13}C NMR resonances for the carbon atoms close to the Rh center in **1** indicates that, in toluene solution, the Li^+ cation is close to Rh as well.

$^1H\{^7Li\}$ NOEs Study of the $[Rh(CH_2CMe_2CH_2CH{=}CH_2)_2]^-$ Anion. To obtain additional information about the relative locations of the Rh and Li centers in solution, we measured the heteronuclear $^1H\{^7Li\}$ nuclear Overhauser enhancements (NOEs) of **1** at −40 °C in toluene-d_8 in a similar fashion as reported elsewhere[68] (Figure S4.15). The measured NOEs are as follows: equatorial α-CH_2 (1.5%), axial α-CH_2 (similar, although quantification is difficult owing to overlap with the methyl resonances of diethyl ether), olefinic methine (0.09%), and olefinic methylene trans to the methine proton (0.06%). Except for the equatorial α-CH_2 group, protons in equatorial positions show essentially no NOEs. This behavior is consistent with the small degree of line broadening of the ^{1}H NMR resonances for the equatorial groups seen at low temperatures and the conclusion that these protons are not close to Li^+.

https://doi.org/10.1021/acs.inorgchem.1c00737
Inorg. Chem. 2021, 60, 8790−8801

Scheme 2. Possible Conformations of 1 in Toluene

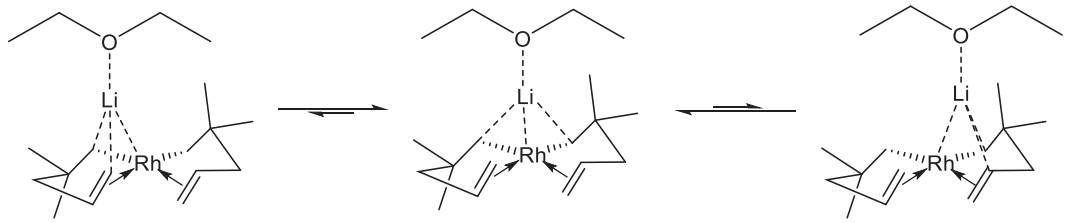

NOEs generally decrease with increasing internuclear separation, and steady-state NOEs can be used to obtain relative distance information. The large NOEs for the α-CH_2 protons clearly demonstrate that, in solution, the Li^+ cation in **1** is closest to these protons. The smaller but nonzero NOEs seen for the olefinic protons in **1**, however, suggest that Li^+ is somewhat further away from these atoms. The location of the Li^+ cation in the vicinity of both the α-CH_2 protons and the olefinic protons suggests that Li^+ must also be in the vicinity of the d_{z^2} orbital of Rh. The deduced structure for **1** is similar to that seen for $[Li(TMEDA)][(COD)Rh(CH_2SiMe_3)_2]$,[31] in which the Li^+ cation interacts primarily with the two α-carbon atoms.

In the solid-state structure of **2**, the two protons that are closest to Li^+ are the axial α-CH_2 (Li−H = 2.05(3) Å) and olefinic methylene proton trans to the methine proton (Li−H = 2.27(3) Å). Both distances are much shorter than the average Li−H distance of 2.93(4) Å and the shortest Li−H distance of 2.85(2) Å for the equatorial α-CH_2 atoms. If a similar structure is adopted by **1** in solution, then we would expect the NOEs for the axial and equatorial α-CH_2 protons to be quite different. Instead, they are similar. One explanation for the similar NOEs for these two protons is the equilibrium shown in Scheme 2 (along with additional equilibria in which the Li^+ cation moves to the opposite face of the Rh square plane).

Computational Studies of the Interactions between Li^+ and the $[Rh(CH_2CMe_2CH_2CH{=}CH_2)_2]^-$ Anion. Both in solution and in the solid state, the Li^+ cation is in close contact with the d_{z^2} orbital of Rh. The apparent interaction between the Li^+ cation and dialkylrhodate anions, $[L_2RhR_2]^-$, and the unusually short Rh−Li distances raise the question whether there are direct rhodium−lithium interactions in these complexes. Two possible models can be used to describe the interactions: (1) the presence of a donor−acceptor bond in which filled d_{z^2} orbitals on rhodium donate to the lithium cation and (2) a simple electrostatic attraction between Li^+ and the negative charge on Rh or its surrounding ligands.

To elucidate the nature of the Rh−Li interactions, we conducted DFT studies based on the crystal structures of **2** and of the previously reported complex $[Li(TMEDA)][(COD)Rh(CH_2SiMe_3)_2]$.[31] A benchmark study was performed using 11 different density functionals to seek the best fit to the experimental crystal structures (SI). The results showed that all of the functionals were able to reproduce the experimental Rh−Li distance within 0.05 Å, but functionals PBE, PBE0, and B3LYP showed the best agreement (within 0.02 Å).

To gain additional insights into the nature of the Rh−Li contact in **2**, we have performed extended-transition-state natural orbital for chemical valence (ETS-NOCV) computations, an energy decomposition scheme that can provide a qualitative picture of chemical bonds. ETS-NOCVs have been extensively applied to characterizing the nature of electron donation and accepting in dative interactions,[79,80] and they offer a computational methodology that can show if the Rh−Li interaction has (weak) dative or electrostatic character. Figure S2 shows the four donor−acceptor NOCV pairs with the largest contribution to the Li interactions in complex **2**. The deformation density ($\Delta\rho$) corresponds to the electron density difference between the donor−acceptor NOCV pair and shows which atoms exhibit electron depletion (blue contours) and which exhibit electron gain (pink contours). Only one of the four deformation densities ($\Delta\rho_2$) corresponds to a Rh−Li interaction (Figure 5). The deformation densities show that the two $4d_{z^2}$ orbitals on Rh are donating electrons to the unoccupied $2p_z$ atomic orbital of Li^+, which can be interpreted as a weak dative bond between the two Rh centers and the Li^+ cation. The ETS-NOCV analysis also revealed a weak coupling of Li^+ with the carbon atoms of the ligand, as was discussed in the previous sections.

Finally, natural energy decomposition analysis (NEDA)[81] calculations were performed to further examine and quantify the strength of the interaction between the Rh centers and the Li^+ cations in **2** and $[Li(TMEDA)][(COD)Rh(CH_2SiMe_3)_2]$. NEDA decomposes the total interaction energy between two or more fragments into a sum of electrical, core, and charge-transfer components. The electrical component comprises two terms, an electrostatic term and a polarization term (which also includes the self-energy correction at each polarizing center). The core component is defined in NEDA as the sum of the

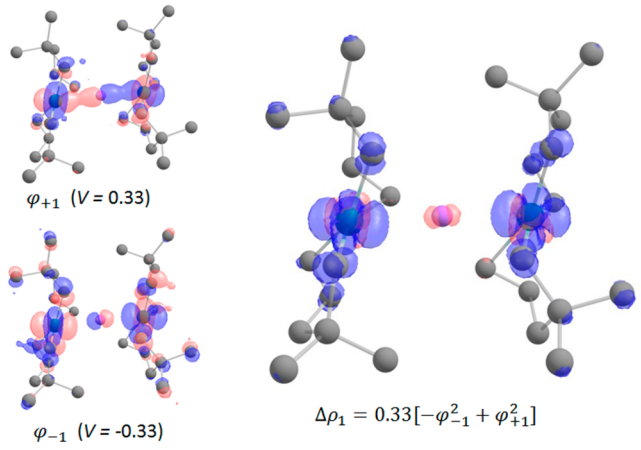

Figure 5. (Left) Extended-transition-state natural orbitals for chemical valence (ETS-NOCV) analysis of the $[Li\{Rh(CH_2CMe_2CH_2CH{=}CH_2)_2\}_2]^-$ anion in **2**. (Right) The difference between the two NOCVs is the net interaction among the three atoms, shown as an electron density difference ($\Delta\rho$). The colors of the deformation densities indicate the flow of electrons from the two Rh centers to Li^+, from blue to pink.

https://doi.org/10.1021/acs.inorgchem.1c00737
Inorg. Chem. 2021, 60, 8790−8801

Table 3. NEDA-Derived Electrical, Core, and Charge-Transfer Contributions to the Total Interaction Energy for Compound 2, Ammonia−Borane, and N_2−Borane[a]

	$[Li\{Rh(CH_2CMe_2CH_2CH{=}CH_2)_2\}_2]^-$	NH_3BH_3	N_2BH_3
electrical	−3961.1	−3185.5	−3393.1
core	3773.8	3369.7	3654.4
charge transfer	−57.0	−229.1	−277.4
total interaction	−244.2	−44.9	−16.1

[a]All energies are in kcal/mol.

exchange and electronic deformation minus the polarization penalty at each center. The charge-transfer term between the two Rh centers and the Li^+ cation in **2** is about one-fifth of the total interaction energy (Table 3). Thus, a weak dative-type interaction is present in **2**, which is in agreement with the ETS-NOCV analysis. For comparison, the charge-transfer term of NH_3BH_3 and N_2BH_3,[82] two representative complexes with dative bond character, is significantly larger than the total interaction energy.

Concluding Remarks. The new alkylrhodate complex $[Li(12\text{-crown-}4)_2][Li\{Rh(CH_2CMe_2CH_2CH{=}CH_2)_2\}_2]$ (**2**) contains the shortest crystallographically characterized Rh−Li contact distances, 2.470(3) and 2.482(3) Å. The short Rh−Li distances persist in nonpolar solvents, as indicated from VT-NMR studies. When dissolved in toluene, the salt $[Li(Et_2O)][Rh(CH_2CMe_2CH_2CH{=}CH_2)_2]$ (**1**) forms an ion pair: a $^1H\{^7Li\}$ NOE NMR study shows that, in solution, the Li^+ cation is in close proximity to the negatively-charged carbon atoms of the pentenyl ligand and, by inference, the d_{z^2} orbital of rhodium.

The short Li−Rh contact distances observed crystallographically in **2** and deduced for **1** in solution were analyzed theoretically. ETS-NOCVs based on DFT calculations showed that electron density is transferred from the $4d_{z^2}$ orbitals of the two Rh centers to the $2p_z$ orbital of Li^+, consistent with the presence of a weak coordinate (dative) bond between Rh and Li. In **2**, the net electron transfer from the two metals to the Li atom is $0.33e^-$, which, based on symmetry considerations, corresponds to $0.165e^-$ per Rh−Li interaction. The charge-transfer term between Li^+ and the two Rh centers contributes only about one-fifth of the total interaction energy, however, and the results are consistent with an earlier proposal that the principal driving force for the proximity of Rh and Li in compounds **1** and **2** is the electrostatic attraction of Li^+ to negative charges on the dialkylrhodiate anions.[31,66]

EXPERIMENTAL SECTION

All experiments were carried out in a vacuum or under argon using standard Schlenk techniques unless otherwise specified. All glassware was oven-dried before use. Pentane and diethyl ether were distilled from sodium/benzophenone, and toluene was distilled from sodium before use. $Rh_2Cl_2(CH_2{=}CH_2)_4$ was prepared by a modification of a literature method (SI).[83] (2,2-Dimethylpent-4-en-1-yl)lithium was prepared as described elsewhere.[68] Toluene-d_8 was purchased from Cambridge Isotope Laboratories and distilled from sodium/benzophenone under nitrogen.

The 1D ^1H, ^6Li, ^7Li, ^{13}C NMR, $^1H-^1H$ COSY, $^1H-^{13}C$ HSQC, and $^1H-^7Li$ NOE data were recorded on a Varian Inova 600 spectrometer at 14.09 T. Chemical shifts are reported in δ units (positive shifts to higher frequency) relative to TMS (^1H, ^{13}C), set by assigning appropriate shifts to residual solvent signals or to an external standard of 1.0 M LiCl (^7Li) by sample replacement. The ^1H and ^{13}C NMR resonances were assigned by analysis of the peak patterns, coupling constants, $^1H-^1H$ COSY, and $^1H-^{13}C$ HSQC spectra. X-ray crystallographic data were collected by the staff of the G. L. Clark X-ray Laboratory at the University of Illinois.

(Diethyl ether)lithium *cis*-Bis(η^1,η^2-2,2-dimethylpent-4-en-1-yl)rhodate(I) (1). To a suspension of $Rh_2Cl_2(CH_2{=}CH_2)_4$ (0.096 g, 0.25 mmol) in diethyl ether (20 mL) at −78 °C was added dropwise a solution of (2,2-dimethylpent-4-en-1-yl)lithium (0.102 g, 0.98 mmol) in pentane (10 mL). A bright-orange solution formed in 5 min. The mixture was stirred at −78 °C for 1 h and then placed in a −50 °C ethanol/glycol bath and stirred for an additional 30 min. The cooling bath was removed and the solvents were removed under vacuum to give a dark oil. (Note that the incomplete removal of solvent gives low yields of product owing to the retention of ethylene, whereas extended evacuation also gives low yields owing to thermal decomposition. Therefore, the next step should be performed immediately after the solvents are removed.) The oil was cooled to −78 °C and was extracted with cold (ca. 0 °C) pentane (15 mL). While the source flask was kept at −78 °C, the red extract was quickly filtered into a cooled (−78 °C) receiver. Rapid evaporation of pentane under vacuum gave a dark oil, which consists of **1** along with small amounts of pentane and silicone grease. The product should be stored in a freezer.

Even in the absence of air and water, **1** decomposes in toluene within several hours at 20 °C into colloidal rhodium, isomers of 4,4-dimethylpentene, and other minor organic byproducts. Because of the thermal instability of **1**, satisfactory elemental analyses and ESI mass spectra could not be obtained. To determine the composition of **1** and estimate the yield, the product from one synthetic run (on the scale given above) was dissolved in toluene-d_8, warmed to room temperature, and exposed to air overnight. The solvent was evaporated by heating the mixture on a hot plate, and the resulting black solid was collected and dried under vacuum to give a free-flowing black powder (49.5 mg). Elemental analysis of this black powder showed 36.6% Rh, 2.14% Li, and 0.33% Cl. From these data, we can conclude that (1) the Rh/Li atomic ratio in the powder is 1:0.9 and is therefore likely to be 1:1 in **1**, (2) the Rh/Cl ratio in the powder is 1:0.026 so that **1** is essentially free of chloride, and (3) the amount of rhodium in the black powder is 0.18 mmol, which suggests that the yield of **1** is ca. 35%. The ^1H NMR spectrum of **1** in toluene-d_8 at −42 °C is consistent with there being one diethyl ether molecule for every two pentenyl ligands (i.e., one diethyl ether molecule per lithium).

$^7Li\{^1H\}$ NMR (233 MHz, C_7D_8, 20 °C): δ 0.40 (s). ^1H NMR (600 MHz, C_7D_8, 20 °C): δ 4.06 (m, 2H, −CH═), 3.20 (d, 2H, $^3J_{HH}$ = 12.3 Hz, ═CH_2, trans to methine), 3.02 (q, 5.2H, $^3J_{HH}$ = 7.0 Hz, −OCH_2 of diethyl ether), 2.41 (d, 2H, $^3J_{HH}$ = 7.7 Hz, ═CH_2, cis to methine), 2.18 (ddd, $^2J_{HH}$ = 12.3 Hz, $^3J_{HH}$ = 5.9 Hz, $^4J_{HH}$ = 2.7 Hz, 2H, γ-CH_2 equatorial), 1.56 (br dd, $^2J_{HH}$ = 12.2 Hz, $^3J_{HH}$ = 8.1 Hz, 2H, γ-CH_2 axial), 1.50 (s, 6H, β-Me axial), 1.26 (s, 6H, β-Me equatorial), 0.94 (s, 7.6H, $^3J_{HH}$ = 7.1 Hz, −CH_3 of diethyl ether), 0.75 (d, 2H, $^2J_{HH}$ = 12.2 Hz, α-CH_2 axial), 0.68 (dd, $^2J_{HH}$ = 11 Hz, $^4J_{HH}$ = 2.7 Hz, 2H, α-CH_2 equatorial). $^{13}C\{^1H\}$ NMR (126 MHz, C_7D_8, 20 °C): δ 77.78 (br, −CH═), 70.90 (br, ═CH_2), 66.35 (s, −OCH_2 of diethyl ether), 51.17 (s, γ-CH_2), 49.12 (s, β-C), 46.71 (br d, $^1J_{RhC}$ = 24 Hz, α-CH_2), 34.33 (s, β-Me axial), 33.13 (s, β-Me equatorial), 14.68 (s, −CH_3 of diethyl ether).

The ^1H NMR peaks broaden at low temperature, and the broadening is greater if the corresponding nucleus is closer to lithium. ^1H NMR (600 MHz, C_7D_8, −40 °C): δ 4.15 (br, 2H, −CH═), 3.29 (br, 2H, ═CH_2, trans to methine), 2.78 (br, 4.5H,

https://doi.org/10.1021/acs.inorgchem.1c00737
Inorg. Chem. 2021, 60, 8790−8801

$-OCH_2$ of diethyl ether), 2.50 (d, 2 H, $^3J_{HH}$ = 7.6 Hz, $=CH_2$, cis to methine), 2.28 (m, 2H, γ-CH_2 equatorial), 1.67 (br dd, $^2J_{HH} \approx 9$ Hz, $^3J_{HH} \approx 9$ Hz, 2H, γ-CH_2 axial), 1.57 (br, 6H, β-Me axial), 1.37 (s, 6H, β-Me equatorial), 0.78 (br, ~6H, $-CH_3$ of diethyl ether), ~0.84 (br, 2H, α-CH_2 axial, overlapping with the methyl group of diethyl ether), 0.68 (d, $^2J_{HH}$ = 8 Hz, 2H, α-CH_2 equatorial). $^{13}C\{^1H\}$ NMR (126 MHz, C_7D_8, −40 °C): δ 66.32 (s, $-OCH_2$ of diethyl ether), 50.87 (br, γ-CH_2), 48.95 (vb, β-C), 34.35 (s, $^3J_{PtC}$ = 99.6 Hz, β-Me equatorial), 33.12 (br, β-Me axial), 14.47 (s, $-CH_3$ of diethyl ether). The resonances corresponding to the α-CH_2 and olefinic carbon atoms are too broad to be observed at this temperature.

Bis(12-crown-4)lithium Bis[*cis*-bis(η^1,η^2-2,2-dimethylpent-4-en-1-yl)rhodate(I)]lithium (2). To a suspension of $[Rh_2Cl_2(CH_2{=}CH_2)_4]$ (0.15g, 0.38 mmol) in diethyl ether (20 mL) at −78 °C was added dropwise a solution of (2,2-dimethylpent-4-en-1-yl)lithium (0.17 g, 1.6 mmol) in pentane (20 mL). The mixture, which turned bright orange in 5 min, was stirred at −78 °C for 2 h and then warmed to −20 °C and stirred at this temperature for 2 h. The reaction flask was evacuated at −20 °C for 5 min to remove the evolved ethylene. The mixture was cooled to −78 °C and filtered into a cooled (−78 °C) receiver; the filtrate was treated with a cooled (−20 °C) solution of 12-crown-4 (0.18 g, 1.0 mmol) in diethyl ether (10 mL) with stirring. An orange precipitate formed immediately. The mixture was warmed to −20 °C and filtered, and the orange solid was extracted with diethyl ether (3 × 10 mL). The filtrates and extracts were combined and slowly evaporated at −20 °C to afford the product as orange prisms. Anal. Calcd for $C_{22}H_{42}Li_2O4RhCl$: C, 50.5; H, 8.10. Found: C, 48.6; H, 8.18. Note that we have been unable to synthesize **2** reproducibly owing to its low thermal stability and high chemical sensitivity (it decomposes when mixed with hydrocarbons such as toluene and Nujol); these properties prevented further characterization by IR or NMR spectroscopy.

Crystallographic Studies. Single crystals of **2** were mounted on glass fibers with Paratone-N oil (Exxon) and immediately cooled to −100 °C in a cold nitrogen gas stream on the diffractometer. Standard peak search and indexing procedures gave rough cell dimensions, and least-squares refinement using 63 318 reflections yielded the cell dimensions given in Table 1.

Data were collected with an area detector by using the measurement parameters listed in Table 1. The monoclinic lattice and systematic absences uniquely suggested space group $P2_1/c$, which was confirmed by the success of the subsequent refinement. The measured intensities were reduced to structure factor amplitudes and their estimated standard deviations by correction for background, scan speed, and Lorentz and polarization effects. No corrections for crystal decay were necessary, but a face-indexed absorption correction was applied, with the minimum and maximum transmission factors being 0.9142 and 0.9695. Systematically absent reflections were deleted and symmetry-equivalent reflections were averaged to yield the set of unique data. Two reflections (1 0 2, 0 2 0) were obscured by the beam stop and were deleted; the remaining 10 418 unique reflections were used in the least-squares refinement.

Intensity data were collected on a Bruker D8 Venture kappa diffractometer equipped with a Photon 100 CMOS detector. An Iμs microfocus source provided the Mo Kα radiation (λ = 0.71073 Å), which was monochromated with multilayer mirrors. The collection, cell refinement, and integration of intensity data were carried out with the APEX3 software.[84] Face-indexed absorption corrections were performed numerically with SADABS.[85] The initial structure solution was solved by direct methods and refined with full-matrix least-squares program SHELXL.[86] Correct positions for the non-hydrogen atoms were deduced from an E-map and subsequent least-squares refinement and difference Fourier calculations. One of the 12-crown-4 rings in the bis(12-crown-4)lithium cation is disordered over two conformations; a site occupancy factor for the major conformer refined to 0.55. The quantity minimized by the least-squares program was $\Sigma w(F_o^2 - F_c^2)^2$, where $w = \{[\sigma(F_o^2)]^2 + (0.0084P)^2 + 4.8998P\}^{-1}$ and $P = (F_o^2 + 2F_c^2)/3$. The analytical approximations to the scattering factors were used, and all structure factors were corrected for both the real and imaginary components of anomalous dispersion. In the final least-squares cycle, independent anisotropic displacement factors were refined for the non-hydrogen atoms. The C−O bond lengths of the disordered crown ether were constrained to an ideal value (1.425 Å) using the DFIX restraint. Hydrogen atoms on the α carbon and the olefinic carbons were located in the difference maps and refined independently. The other hydrogen atoms were placed in idealized positions; the methyl groups were allowed to rotate about the C−C axis to find the best least-squares positions. The displacement parameters for methylene and methine hydrogens were set equal to $1.2U_{eq}$ for the attached carbon; those for methyl hydrogens were set to $1.5U_{eq}$. An isotropic extinction parameter was refined to a final value of $x = 3.55(8) \times 10^{-6}$, where F_c is multiplied by the factor $k[1 + F_c^2 x\lambda^3/\sin 2\theta]^{-1/4}$, with k being the overall scale factor. Successful convergence was indicated by the maximum shift/error of 0.003 for the last cycle. Final refinement parameters are given in Table 1. The largest peak in the final Fourier difference map (0.64 eÅ^{-3}) was located 1.66 Å from Li2. A final analysis of variance between observed and calculated structure factors showed no apparent errors.

NOE NMR Experiments. NOE experiments were performed at −40 °C on solutions of **1** (~0.7 M) in C_7D_8 placed in flame-sealed NMR tubes. The resonance due to the equatorial α-CH_2 protons, which is well separated from other resonances, shows a relatively large NOE of 1.5%. The NOEs for the other resonances (most of which are smaller) were determined by a comparison of the difference peak integral with that of the equatorial α-CH_2 proton. The $^7Li-^1H$ NOE difference spectrum was obtained by subtracting a standard ^1H spectrum from the ^1H spectrum collected after saturating the ^7Li resonance for 5 s, with a recycle delay of 2.0 s.

Computational Details. Structural optimizations were performed with the Gaussian 09 program package[87] with density functional theory (DFT), Grimme's D3 empirical dispersion correction,[88] and the Becke−Johnson damping function.[89] A full list of density functionals tested in this study is given in the Supporting Information. The def2-TZVP[90] basis set was used for all atoms except Rh. For Rh, an additional polarization function was added (def2-TZVPP[90] basis set), and the core electrons were treated with the SDD effective core potential.[91] The minimum-energy structures calculated with the PBE-D3(BJ) and PBE0 functionals showed the greatest geometrical similarity of the Rh−Li−Rh unit to that seen in the crystal structure of **2**. Because of the large steric bulk of the surrounding ligands, the dispersion corrections at the PBE level provide increased accuracy. For all optimized structures with bond lengths within 0.02 Å of the crystal structure, a frequency calculation was performed to ensure that the optimized geometry was at a minimum rather than a saddle point on the potential energy surface.

Extended-transition-state natural orbitals for chemical valence (ETS-NOCV)[92] were computed with the ORCA 4.2.0 package[93] using the def2-QZVP[90] basis set and SDD electron core potentials[91] for the rhodium atoms and def2-TZVP for all other atoms. The NOCV method partitions the interaction energy into meaningful contributions and provides a qualitative picture of electron donations and back-donations. Two different fragmentation schemes for **2** were considered in the ETS-NOCV computations. The first scheme considers the Li atom to be the first fragment (subsystem) whereas all of the other atoms constitute the second fragment. The second scheme considers one Rh-ligand complex to be the first fragment, whereas the Li atom together with the second Rh-ligand complex is the second fragment. A detailed analysis is provided in the Supporting Information. All ETS-NOCV calculations were performed with the range-separated hybrid density functional ωB97x-D3(BJ).[94−96]

Natural energy decomposition analysis (NEDA)[81] calculations were performed as implemented in the NBO7.0[97] software and interfaced with Gaussian 16.[98] NEDA calculations were performed with a natural bond orbital (NBO) basis, the long-range ωB97XD density functional, and the def2-TZVP basis set. The NEDA method was used to study **2** as well as two model molecular compounds with dative bonds (NH_3BH_3 and N_2BH_3).

https://doi.org/10.1021/acs.inorgchem.1c00737
Inorg. Chem. 2021, 60, 8790−8801

■ ASSOCIATED CONTENT

Supporting Information

The Supporting Information is available free of charge at https://pubs.acs.org/doi/10.1021/acs.inorgchem.1c00737.

^{1}H, ^{6}Li, ^{7}Li, ^{13}C, COSY, HSQC, and ^{1}H{^{7}Li} NOE NMR spectra of **1**; full list of bond distances and bond angles for **2**, along with details of the benchmark DFT calculations; NBO analysis; and ETS-NOCV analysis (PDF)

Accession Codes

CCDC 2069183 contains the supplementary crystallographic data for this paper. These data can be obtained free of charge via www.ccdc.cam.ac.uk/data_request/cif, or by emailing data_request@ccdc.cam.ac.uk, or by contacting The Cambridge Crystallographic Data Centre, 12 Union Road, Cambridge CB2 1EZ, UK; fax: +44 1223 336033.

■ AUTHOR INFORMATION

Corresponding Authors

Gregory S. Girolami − *School of Chemical Sciences, University of Illinois at Urbana−Champaign, Urbana, Illinois 61801, United States;* orcid.org/0000-0002-7295-1775; Email: girolami@scs.illinois.edu

Konstantinos D. Vogiatzis − *Department of Chemistry, University of Tennessee, Knoxville, Tennessee 37996, United States;* orcid.org/0000-0002-7439-3850; Email: kvogiatz@utk.edu

Authors

Sumeng Liu − *School of Chemical Sciences, University of Illinois at Urbana−Champaign, Urbana, Illinois 61801, United States;* Present Address: (S.L.) Department of Chemistry, University of California at Riverside, Riverside, California 92521, United States.; orcid.org/0000-0002-2133-2122

Brett A. Smith − *Department of Chemistry, University of Tennessee, Knoxville, Tennessee 37996, United States;* orcid.org/0000-0003-0258-9704

Justin K. Kirkland − *Department of Chemistry, University of Tennessee, Knoxville, Tennessee 37996, United States*

Complete contact information is available at: https://pubs.acs.org/10.1021/acs.inorgchem.1c00737

Funding

National Science Foundation under grants CHE 1954745 and CHE 1665191 (to G.S.G.) and CHE-1800237 (to K.D.V.).

Notes

The authors declare no competing financial interest.

■ ACKNOWLEDGMENTS

G.S.G. thanks the National Science Foundation (grants CHE 16-65191 and CHE 19-54745) for supporting this research. B.A.S., J.K.K., and K.D.V. gratefully acknowledge the National Science Foundation (CHE-1800237) for financially supporting this work and the Advanced Computer Facility (ACF) of the University of Tennessee for computational resources.

■ REFERENCES

(1) Berry, J. F.; Lu, C. C. Metal-Metal Bonds: From Fundamentals to Applications. *Inorg. Chem.* **2017**, *56*, 7577−7581.

(2) Wheatley, N.; Kalck, P. Structure and Reactivity of Early-Late Heterobimetallic Complexes. *Chem. Rev.* **1999**, *99*, 3379−3420.

(3) Buchwalter, P.; Rosé, J.; Braunstein, P. Multimetallic Catalysis Based on Heterometallic Complexes and Clusters. *Chem. Rev.* **2015**, *115*, 28−126.

(4) Eisenhart, R. J.; Clouston, L. J.; Lu, C. C. Configuring Bonds between First-Row Transition Metals. *Acc. Chem. Res.* **2015**, *48*, 2885−2894.

(5) Moore, J. T.; Chatterjee, S.; Tarrago, M.; Clouston, L. J.; Sproules, S.; Bill, E.; Bernales, V.; Gagliardi, L.; Ye, S.; Lancaster, K. M.; Lu, C. C. Enhanced Fe-Centered Redox Flexibility in Fe-Ti Heterobimetallic Complexes. *Inorg. Chem.* **2019**, *58*, 6199−6214.

(6) Greenwood, B. P.; Rowe, G. T.; Chen, C.-H.; Foxman, B. M.; Thomas, C. M. Metal-Metal Multiple Bonds in Early/Late Heterobimetallics Support Unusual Trigonal Monopyramidal Geometries at both Zr and Co. *J. Am. Chem. Soc.* **2010**, *132*, 44−45.

(7) Krogman, J. P.; Gallagher, J. R.; Zhang, G.; Hock, A. S.; Miller, J. T.; Thomas, C. M. Assignment of the Oxidation States of Zr and Co in a Highly Reactive Heterobimetallic Zr/Co Complex Using X-ray Absorption Spectroscopy (XANES). *Dalton Trans.* **2014**, *43*, 13852−13857.

(8) Gramigna, K. M.; Dickie, D. A.; Foxman, B. M.; Thomas, C. M. Cooperative H_2 Activation across a Metal-Metal Multiple Bond and Hydrogenation Reactions Catalyzed by a Zr/Co Heterobimetallic Complex. *ACS Catal.* **2019**, *9*, 3153−3164.

(9) Coombs, J.; Perry, D.; Kwon, D.-H.; Thomas, C. M.; Ess, D. H. Why Two Metals Are Better Than One for Heterodinuclear Cobalt-Zirconium-Catalyzed Kumada Coupling. *Organometallics* **2018**, *37*, 4195−4203.

(10) Wu, B.; Gramigna, K. M.; Bezpalko, M. W.; Foxman, B. M.; Thomas, C. M. Heterobimetallic Ti/Co Complexes That Promote Catalytic N-N Bond Cleavage. *Inorg. Chem.* **2015**, *54*, 10909−10917.

(11) Fürstner, A.; Krause, H.; Lehmann, C. W. Unusual Structure and Reactivity of a Homoleptic "Super-Ate" Complex of Iron: Implications for Grignard Additions, Cross-Coupling Reactions, and the Kharasch Deconjugation. *Angew. Chem., Int. Ed.* **2006**, *45*, 440−444.

(12) Fürstner, A.; Martin, R.; Krause, H.; Seidel, G.; Goddard, R.; Lehmann, C. W. Preparation, Structure, and Reactivity of Nonstabilized Organoiron Compounds. Implications for Iron-Catalyzed Cross Coupling Reactions. *J. Am. Chem. Soc.* **2008**, *130*, 8773−8787.

(13) Nattmann, L.; Lutz, S.; Ortsack, P.; Goddard, R.; Cornella, J. A Highly Reduced Ni-Li-Olefin Complex for Catalytic Kumada-Corriu Cross-Couplings. *J. Am. Chem. Soc.* **2018**, *140*, 13628−13633.

(14) Buchalski, P.; Pacholski, R.; Gustowski, J.; Buchowicz, W.; Molga, K.; Shkurenko, A.; Suwińska, K. Bis-nickel-bridged *p*-Terphenyl Dianion - Synthesis and Structures. *J. Organomet. Chem.* **2015**, *789*−*790*, 40−45.

(15) Fürstner, A.; Martin, R.; Majima, K. Cycloisomerization of Enynes Catalyzed by Iron(0)-Ate Complexes. *J. Am. Chem. Soc.* **2005**, *127*, 12236−12237.

(16) Fürstner, A.; Majima, K.; Martín, R.; Krause, H.; Kattnig, E.; Goddard, R.; Lehmann, C. W. A Cheap Metal for a "Noble" Task: Preparative and Mechanistic Aspects of Cycloisomerization and Cycloaddition Reactions Catalyzed by Low-Valent Iron Complexes. *J. Am. Chem. Soc.* **2008**, *130*, 1992−2004.

(17) Pörschke, K.-R.; Jonas, K.; Wilke, G.; Benn, R.; Mynott, R.; Goddard, R.; Krüger, C. Zur Lewis-Acidität von Nickel(0), I. Methyllithium-Komplexe von Nickel(0). *Chem. Ber.* **1985**, *118*, 275−297.

(18) Poverenov, E.; Gandelman, M.; Shimon, L. J. W.; Rozenberg, H.; Ben-David, Y.; Milstein, D. Nucleophilic De-coordination and Electrophilic Regeneration of "Hemilabile" Pincer-Type Complexes: Formation of Anionic Dialkyl, Diaryl, and Dihydride Pt^{II} Complexes Bearing No Stabilizing π-Acceptors. *Chem. - Eur. J.* **2004**, *10*, 4673−4684.

(19) Fröhlich, H.-O.; Wyrwa, R.; Görls, H. Synthesis, Properties, and Structure of — A New Type of Pt^{II} Metallacyclopentane Complexes. *Angew. Chem., Int. Ed. Engl.* **1993**, *32*, 387−388.

(20) Fröhlich, H.-O.; Wyrwa, R.; Görls, H.; Pieper, U. Beiträge zur Chemie Organometallischer Metallacyclischer Nebengruppenmetall-

verbindungen: IX. Eine Ungewöhnliche Koordinationsgeometrie des Platin(II) in dem Homoleptischen Metallacyclopentankomplex $[Li(PMDETA)]_2Pt(CH_2CH_2CH_2CH_2)_2$. *J. Organomet. Chem.* **1994**, *471*, 23−27.
(21) Sebald, A.; Wrackmeyer, B.; Theocharis, C. R.; Jones, W. Reactions of Platinum(II) Acetylides with Organolithium Compounds: Formation of Lithium-bridged Dinuclear Platinum(II) Complexes and of Triorganoplatinate(II) Complexes: Crystal Structure of the Complex $[Pt_2(C{\equiv}CPh)_4(PEt_3)_2(Bu^n)_2(\mu\text{-}Li)_2]$. *J. Chem. Soc., Dalton Trans.* **1984**, 747−756.
(22) Wyrwa, R.; Görls, H. Ungewöhnliche Molekülstrukturen für Platin(II)-at-Komplexe. *Z. Anorg. Allg. Chem.* **1999**, *625*, 1904−1907.
(23) Jonas, K.; Krüger, C. Alkali Metal-Transition Metal π-Complexes. *Angew. Chem., Int. Ed. Engl.* **1980**, *19*, 520−537.
(24) Buchalski, P.; Grabowska, I.; Kamińska, E.; Suwińska, K. Synthesis and Structures of 9-Nickelafluorenyllithium Complexes. *Organometallics* **2008**, *27*, 2346−2349.
(25) Fröhlich, H.-O.; Wyrwa, R.; Görls, H. Beiträge zur Chemie Organometallischer Metallacyclischer Nebengruppenmetallverbindungen: V. Synthese von Li_2 $Ni(CH_2CH_2CH_2CH_2)_2(Solv)_x$ aus $K[Ni(NPh_2)_3](THF)$ und $LiCH_2CH_2CH_2CH_2Li$; Molekülstruktur von $(Li(THF)_2)_2$ $Ni(CH_2CH_2CH_2CH_2)_2$. *J. Organomet. Chem.* **1992**, *441*, 169−175.
(26) Wyrwa, R.; Fröhlich, H.-O.; Görls, H. Beiträge zur Chemie Organometallischer Metallacyclischer Nebengruppenmetallverbindungen XII. Synthese, NMR-spektroskopische Untersuchung und Kristallstruktur von $[Li(PMDETA)]_2Ni(CH_2CH_2CH_2CH_2)_2$ 1— Vergleichende DTA-Untersuchungen von 1 und Unsubstituierten Nickelacyclopentan-Komplexen der Zusammensetzung $[LiL_x]_2Ni(CH_2CH_2CH_2CH_2)_2$ (L = TMEDA, THF, d_8-THF). *J. Organomet. Chem.* **1995**, *491*, 41−46.
(27) Goddard, R.; Krüger, C.; Pörschke, K. R.; Wilke, G. Elektronendichte-Verteilungen in Metallorganischen Verbindungen. Wechselnde Struktur- und Bindungsverhältnisse in Dimeren Metallorganischen Nickel-Hydriden mit Ionenpaar-Beziehungen zu den Hauptgruppen-Metallen Natrium und Lithium. *J. Organomet. Chem.* **1986**, *308*, 85−103.
(28) Steinborn, D.; Becke, F.; Boese, R. Synthesis and Properties of (Aminomethyl)nickel Complexes. $[\{Li(OEt_2)\}_2Ni(CH_2NC_5H_{10})_4]$: The First Structurally Characterized Homoleptic Aminomethyl Complex of a Transition Metal. *Inorg. Chem.* **1995**, *34*, 2625−2628.
(29) Fröhlich, H.-O.; Wyrwa, R.; Görls, H. Beiträdge zur Chemie Organometallischer Metallacyclischer Nebengruppenmetallverbindungen: VIII. Synthese und Eigenschaften von $Li_2Pd(CH_2(CH_2)_2CH_2)_2(D)_x$ Molekülstruktur von $[Li(THF)_2]_2Pd(CH_2(CH_2)_2CH_2)_2$. *J. Organomet. Chem.* **1993**, *456*, 7−12.
(30) Fryzuk, M. D.; Lloyd, B. R.; Clentsmith, G. K. B.; Rettig, S. J. Binuclear Palladium Complexes with Bridging Hydrides. Unusual Coordination Behavior of $LiBEt_4$ and $NaBEt_4$. *J. Am. Chem. Soc.* **1994**, *116*, 3804−3812.
(31) Kulzick, M. A.; Andersen, R. A.; Muetterties, E. L.; Day, V. W. Bridging Alkyls in *d*-Transition Metal Chemistry: Reactions of $(cod)_2M_2(\mu\text{-}R)_2$ with Organolithium Reagents to Give $(cod)_2M_2(R)_4Li_2$, where M is Rh or Ir, and the Crystal Structure of $(cod)_2Rh_2(CH_2SiMe_3)_4Li_2$ and $(cod)Rh(CH_2SiMe_3)_2Li(Me_2NCH_2CH_2NMe_2)$. *J. Organomet. Chem.* **1987**, *336*, 221−236.
(32) Bönnemann, H.; Krüger, C.; Tsay, Y.-H. A Lithium-Cobalt Bimetal Complex. *Angew. Chem., Int. Ed. Engl.* **1976**, *15*, 46−47.
(33) Alexander, C. S.; Rettig, S. J.; James, B. R. Synthesis and Structural Characterization of (Neopentyl)(octaethylporphyrinato) ruthenium Complexes, Including $[Ru(OEP)Np]_2(\mu\text{-}Li)_2$. *Organometallics* **1994**, *13*, 2542−2544.
(34) Bazhenova, T. A.; Kachapina, L. M.; Shilov, A. E.; Antipin, M. Y.; Struchkov, Y. T. Mono- and Binuclear σ-Aryl Iron-Lithium Hydrides; Synthesis and Molecular Structure. *J. Organomet. Chem.* **1992**, *428*, 107−123.
(35) Al-Ktaifani, M. M.; Hitchcock, P. B.; Nixon, J. F. Lithiation and Alkylation Reactions of the Tri-phosphaferrocenes, $[Fe(\eta^5\text{-}P_3C_2{}^tBu_2)(\eta^5\text{-}C_5R_5)]$, (R = H and Me): Crystal and Molecular Structures of the $LiFe(\eta^4\text{-}P_2C_2{}^tBu_2P^nBu)(\eta^5\text{-}C_5Me_5)_2$ dimer, $[Fe(\eta^4\text{-}P_2C_2{}^tBu_2P^nBuMe)(\eta^5\text{-}C_5Me_5)]$ and *cis*-$[PtCl_2(PMe_3)Fe(\eta^4\text{-}P_2C_2{}^tBu_2P^nBuMe)(\eta^5\text{-}C_5H_5)]$. *J. Organomet. Chem.* **2008**, *693*, 611−618.
(36) Casitas, A.; Krause, H.; Lutz, S.; Goddard, R.; Bill, E.; Fürstner, A. Ligand Exchange on and Allylic C-H Activation by Iron(0) Fragments: π-Complexes, Allyliron Species, and Metallacycles. *Organometallics* **2018**, *37*, 729−739.
(37) Iwasaki, T.; Akaiwa, T.; Hirooka, Y.; Pal, S.; Nozaki, K.; Kambe, N. Synthesis of and Structural Insights into Contact Ion Pair and Solvent-Separated Ion Pair Diphenyliridate Complexes. *Organometallics* **2020**, *39*, 3077−3081.
(38) Ekkert, O.; White, A. J. P.; Toms, H.; Crimmin, M. R. Addition of Aluminium, Zinc and Magnesium Hydrides to Rhodium(III). *Chem. Sci.* **2015**, *6*, 5617−5622.
(39) Golden, J. T.; Peterson, T. H.; Holland, P. L.; Bergman, R. G.; Andersen, R. A. Adduct Formation and Single and Double Deprotonation of $Cp^*(PMe_3)Ir(H)_2$ with Main Group Metal Alkyls and Aryls: Synthesis and Structure of Three Novel Ir-Al and Ir-Mg Heterobimetallics. *J. Am. Chem. Soc.* **1998**, *120*, 223−224.
(40) Lau, S.; White, A. J. P.; Casely, I. J.; Crimmin, M. R. Tunable Binding of Dinitrogen to a Series of Heterobimetallic Hydride Complexes. *Organometallics* **2018**, *37*, 4521−4526.
(41) Ohashi, M.; Matsubara, K.; Iizuka, T.; Suzuki, H. Trinuclear Ruthenium Polyhydride Complexes with a Triply Bridging Ligand: $[\{(\eta^5\text{-}C_5Me_5)Ru\}_3(\mu_3\text{-}M)(\mu\text{-}H)_3(\mu_3\text{-}H)]$ (M = Li, Mg^{i}Pr, and ZnEt) and $[\{(\eta^5\text{-}C_5Me_5)Ru\}_3(\mu_3\text{-}M)(\mu\text{-}H)_3]$ (M = AlEt and GaMe). *Angew. Chem., Int. Ed.* **2003**, *42*, 937−940.
(42) Hounjet, L. J.; Adhikari, D.; Pink, M.; Carroll, P. J.; Mindiola, D. J. Synthesis of an Iron(II) Ethyl Complex Accompanied by Formation of an Unusual Dinitrogen-Ligated Iron(I) Hydride. *Z. Anorg. Allg. Chem.* **2015**, *641*, 45−48.
(43) Blake, M. P.; Kaltsoyannis, N.; Mountford, P. Synthesis and Reactions of β-Diketiminate-supported Complexes with Mg-Fe or Yb-Fe Bonds. *Chem. Commun.* **2013**, *49*, 3315−3317.
(44) Felkin, H.; Knowles, P. J.; Meunier, B.; Mitschler, A.; Ricard, L.; Weiss, R. Preparation and Crystal Structure of π-Cyclopentadienyl-1,2-bis(diphenylphosphino)ethaneironmagnesium Bromide Tris(tetrahydrofuran), a Transition-Metal Grignard Reagent. *J. Chem. Soc., Chem. Commun.* **1974**, 44−44.
(45) Green, R.; Walker, A. C.; Blake, M. P.; Mountford, P. Synthesis, Characterisation and Structural Studies of Amidinate and Guanidinate Alkaline Earth-Transition Metal Bonded Complexes. *Polyhedron* **2016**, *116*, 64−75.
(46) Garçon, M.; Bakewell, C.; White, A. J. P.; Crimmin, M. R. Unravelling Nucleophilic Aromatic Substitution Pathways with Bimetallic Nucleophiles. *Chem. Commun.* **2019**, *55*, 1805−1808.
(47) Blake, M. P.; Kaltsoyannis, N.; Mountford, P. Probing the Limits of Alkaline Earth-Transition Metal Bonding: An Experimental and Computational Study. *J. Am. Chem. Soc.* **2015**, *137*, 12352−12368.
(48) Fohlmeister, L.; Liu, S.; Schulten, C.; Moubaraki, B.; Stasch, A.; Cashion, J. D.; Murray, K. S.; Gagliardi, L.; Jones, C. Low-Coordinate Iron(I) and Manganese(I) Dimers: Kinetic Stabilization of an Exceptionally Short Fe—Fe Multiple Bond. *Angew. Chem., Int. Ed.* **2012**, *51*, 8294−8298.
(49) Jonas, K.; Koepe, G.; Krüger, C. Heterometallic Dinuclear Complexes by Ethene Displacement with Grignard Compounds or Diorganomagnesium Compounds. *Angew. Chem., Int. Ed. Engl.* **1986**, *25*, 923−925.
(50) Wilke, G. Contributions to Organo-Nickel Chemistry. *Angew. Chem., Int. Ed. Engl.* **1988**, *27*, 185−206.
(51) Shoshani, M. M.; Liu, J.; Johnson, S. A. Mechanistic Insight into H/D Exchange by a Pentanuclear Ni-H Cluster and Synthesis and Characterization of Structural Analogues of Potential Intermediates. *Organometallics* **2018**, *37*, 116−126.
(52) Garçon, M.; Bakewell, C.; Sackman, G. A.; White, A. J. P.; Cooper, R. I.; Edwards, A. J.; Crimmin, M. R. A Hexagonal Planar Transition-Metal Complex. *Nature* **2019**, *574*, 390−393.

https://doi.org/10.1021/acs.inorgchem.1c00737
Inorg. Chem. 2021, 60, 8790−8801

(53) Baddour, F. G.; Hyre, A. S.; Guillet, J. L.; Pascual, D.; Lopez-De-Luzuriaga, J. M.; Alam, T. M.; Bacon, J. W.; Doerrer, L. H. Pt-Mg, Pt-Ca, and Pt-Zn Lantern Complexes and Metal-Only Donor-Acceptor Interactions. *Inorg. Chem.* **2017**, *56*, 452−469.
(54) Bauer, J.; Braunschweig, H.; Dewhurst, R. D. Metal-Only Lewis Pairs with Transition Metal Lewis Bases. *Chem. Rev.* **2012**, *112*, 4329−4346.
(55) Brauer, D. J.; Krüger, C.; Sekutowski, J. C. Structural Investigations of Mixed Metal Compounds; the Stereochemistry of Two Dilithium-Tris(olefin)nickel(0) Complexes. *J. Organomet. Chem.* **1979**, *178*, 249−260.
(56) Brauer, D. J.; Krüger, C.; Roberts, P. J.; Tsay, Y.-H. Structure of a Bimetal-Ethylene Complex: $[(C_6H_5)_2NiC_2H_4]_2Na_4(THF)_5$. *Angew. Chem., Int. Ed. Engl.* **1976**, *15*, 48−49.
(57) Kaschube, W.; Pörschke, K.-R.; Angermund, K.; Krüger, C.; Wilke, G. Zur Lewis-Acidität von Nickel(0), X. Diorganylmagnesium-Komplexe von Nickel(0): $(TMEDA)MgCH_3(\mu\text{-}CH_3)Ni(C_2H_4)_2$. *Chem. Ber.* **1988**, *121*, 1921−1929.
(58) Birchall, C.; Moxey, G. J.; McMaster, J.; Blake, A. J.; Lewis, W.; Kays, D. L. A Monomeric, Heterobimetallic Complex with an Unsupported Mg-Fe Bond. *Inorg. Chim. Acta* **2017**, *458*, 97−100.
(59) Moore, J. T.; Smith, N. E.; Lu, C. C. Structure and Dynamic NMR Behavior of Rhodium Complexes Supported by Lewis Acidic Group 13 Metallatranes. *Dalton Trans.* **2017**, *46*, 5689−5701.
(60) Mayer, J. M.; Calabrese, J. C. Reactions of Alkylaluminum Reagents with Basic and Acidic Rhodium Compounds. X-ray Crystal and Molecular Structure of $(\eta\text{-}C_5H_5)Rh(PMe_3)_2(Al_2Me_4Cl_2)$, a Rhodium-Lewis Acid Adduct. *Organometallics* **1984**, *3*, 1292−1298.
(61) Steinke, T.; Gemel, C.; Cokoja, M.; Winter, M.; Fischer, R. A. Novel RhCp*/GaCp* and RhCp*/InCp* Cluster Complexes. *Dalton Trans.* **2005**, 55−62.
(62) Kuppuswamy, S.; Cass, T. R.; Bezpalko, M. W.; Foxman, B. M.; Thomas, C. M. Synthesis and Investigation of the Metal-Metal Interactions in Heterobimetallic Cr/Rh and Cr/Ir Complexes. *Inorg. Chim. Acta* **2015**, *424*, 167−172.
(63) Hlina, J. A.; Wells, J. A. L.; Pankhurst, J. R.; Love, J. B.; Arnold, P. L. Uranium Rhodium Bonding in Heterometallic Complexes. *Dalton Trans.* **2017**, *46*, 5540−5545.
(64) Cordero, B.; Gómez, V.; Platero-Prats, A. E.; Revés, M.; Echeverría, J.; Cremades, E.; Barragán, F.; Alvarez, S. Covalent Radii Revisited. *Dalton Trans.* **2008**, 2832−2838.
(65) Angermund, K.; Claus, K. H.; Goddard, R.; Krüger, C. High-Resolution X-ray Crystallography—An Experimental Method for the Description of Chemical Bonds. *Angew. Chem., Int. Ed. Engl.* **1985**, *24*, 237−247.
(66) Del Paggio, A. A.; Andersen, R. A.; Muetterties, E. L. The Chemistry of Bulky Chelating Phosphines. 3. Anionic Alkyl and Aryl Complexes of Rhodium(I) and Iridium(I). *Organometallics* **1987**, *6*, 1260−1267.
(67) Liu, S.; Zhang, Z.; Gray, D.; Zhu, L.; Abelson, J. R.; Girolami, G. S. Platinum ω-Alkenyl Compounds as Chemical Vapor Deposition Precursors. Synthesis and Characterization of $Pt[CH_2CMe_2CH_2CH = CH_2]_2$ and the Impact of Ligand Design on the Deposition Process. *Chem. Mater.* **2020**, *32*, 9316−9334.
(68) Liu, S.; Gray, D.; Zhu, L.; Girolami, G. S. Lithium-Olefin π-Complexes and the Mechanism of Carbolithiation: Synthesis, Solution Behavior, and Crystal Structure of (2,2-Dimethylpent-4-en-1-yl)lithium. *Organometallics* **2019**, *38*, 2199−2210.
(69) Bennett, M. A.; Hann, E. J. Tetraphenylborate Ion-Promoted Hydrogenation of Planar Rhodium(I) Cations Formed by a Chelating Olefinic Tertiary Phosphine or Arsine. *J. Organomet. Chem.* **1977**, *124*, 213−220.
(70) Zhao, P.; Incarvito, C. D.; Hartwig, J. F. Carbon-Oxygen Bond Formation between a Terminal Alkoxo Ligand and a Coordinated Olefin. Evidence for Olefin Insertion into a Rhodium Alkoxide. *J. Am. Chem. Soc.* **2006**, *128*, 9642−9643.
(71) Krafft, M. E.; Yu, X. Y.; Wilson, L. J. Amine-Directed Alkene Hydrocarboxylation. *Organometallics* **1998**, *17*, 2076−2088.
(72) Clark, P. W.; Hartwell, G. E. Tris-Olefin Complexes of Rhodium(I) and Iridium(I) Containing the Tetradentate Ligands Tris(but-3-enyl)phosphine and Tris(pent-4-enyl)phosphine. *J. Organomet. Chem.* **1975**, *97*, 117−129.
(73) Hall, J. R.; Appleton, T. G. Complexes with Six-Membered Chelate Rings. III. Factors Influencing the Values of the Platinum-Proton Coupling Constants $^3J_{Pt\text{-}N\text{-}C\text{-}H}$ and $^4J_{Pt\text{-}N\text{-}C\text{-}CH3}$ in Diamine Complexes of Platinum(II) and -(IV). *Inorg. Chem.* **1971**, *10*, 1717−1725.
(74) Karplus, M. Contact Electron-Spin Coupling of Nuclear Magnetic Moments. *J. Chem. Phys.* **1959**, *30*, 11−15.
(75) Lindman, B.; Forsén, S. The Alkali Metals. In *NMR and the Periodic Table*; Harris, R. K., Mann, B. E., Eds.; Academic Press: London, 1978; pp 129−175.
(76) Fulmer, G. R.; Miller, A. J. M.; Sherden, N. H.; Gottlieb, H. E.; Nudelman, A.; Stoltz, B. M.; Bercaw, J. E.; Goldberg, K. I. NMR Chemical Shifts of Trace Impurities: Common Laboratory Solvents, Organics, and Gases in Deuterated Solvents Relevant to the Organometallic Chemist. *Organometallics* **2010**, *29*, 2176−2179.
(77) Gasparro, F. P.; Kolodny, N. H. NMR Determination of the Rotational Barrier in N,N-Dimethylacetamide. A Physical Chemistry Experiment. *J. Chem. Educ.* **1977**, *54*, 258.
(78) Buckingham, A. D.; Schaefer, T.; Schneider, W. G. Solvent Effects in Nuclear Magnetic Resonance Spectra. *J. Chem. Phys.* **1960**, *32*, 1227−1233.
(79) Frenking, G.; Fröhlich, N. The Nature of the Bonding in Transition-Metal Compounds. *Chem. Rev.* **2000**, *100*, 717−774.
(80) Jerabek, P.; Schwerdtfeger, P.; Frenking, G. Dative and Electron-Sharing Bonding in Transition Metal Compounds. *J. Comput. Chem.* **2019**, *40*, 247−264.
(81) Glendening, E. D.; Streitwieser, A. Natural Energy Decomposition Analysis: An Energy Partitioning Procedure for Molecular Interactions with Application to Weak Hydrogen Bonding, Strong Ionic, and Moderate Donor-Acceptor Interactions. *J. Chem. Phys.* **1994**, *100*, 2900−2909.
(82) Townsend, J.; Braunscheidel, N. M.; Vogiatzis, K. D. Understanding the Nature of Weak Interactions between Functionalized Boranes and N_2/O_2, Promising Functional Groups for Gas Separations. *J. Phys. Chem. A* **2019**, *123*, 3315−3325.
(83) Cramer, R.; McCleverty, J. A.; Bray, J. Di-μ-chlorotetrakis(ethylene)dirhodium(I), 2,4-Pentanedionatobis(ethylene)rhodium(I), and Di-μ-chlorotetracarbonyldirhodium(I). *Inorg. Synth.* **2007**, *16*, 14−18.
(84) *APEX3*; Bruker AXS, Inc: Madison, WI, 2018.
(85) Krause, L.; Herbst-Irmer, R.; Sheldrick, G. M.; Stalke, D. Comparison of Silver and Molybdenum Microfocus X-ray Sources for Single-Crystal Structure Determination. *J. Appl. Crystallogr.* **2015**, *48*, 3−10.
(86) Sheldrick, G. Crystal Structure Refinement with SHELXL. *Acta Crystallogr., Sect. C: Struct. Chem.* **2015**, *71*, 3−8.
(87) Frisch, M. J. T. G. W.; Schlegel, H. B.; Scuseria, G. E.; Robb, M. A.; Cheeseman, J. R.; Scalmani, G.; Barone, V.; Mennucci, B.; Petersson, G. A.; Nakatsuji, H.; Caricato, M.; Li, X.; Hratchian, H. P.; Izmaylov, A. F.; Bloino, J.; Zheng, G.; Sonnenberg, J. L.; Hada, M.; Ehara, M.; Toyota, K.; Fukuda, R.; Hasegawa, J.; Ishida, M.; Nakajima, T.; Honda, Y.; Kitao, O.; Nakai, H.; Vreven, T.; Montgomery, J. A.; Peralta, J. E.; Ogliaro, F.; Bearpark, M.; Heyd, J. J.; Brothers, E.; Kudin, K. N.; Staroverov, V. N.; Keith, T.; Kobayashi, R.; Normand, J.; Raghavachari, K.; Rendell, A.; Burant, J. C.; Iyengar, S. S.; Tomasi, J.; Cossi, M.; Rega, N.; Millam, J. M.; Klene, M.; Knox, J. E.; Cross, J. B.; Bakken, V.; Adamo, C.; Jaramillo, J.; Gomperts, R.; Stratmann, R. E.; Yazyev, O.; Austin, A. J.; Cammi, R.; Pomelli, C.; Ochterski, J. W.; Martin, R. L.; Morokuma, K.; Zakrzewski, V. G.; Voth, G. A.; Salvador, P.; Dannenberg, J. J.; Dapprich, S.; Daniels, A. D.; Farkas, O.; Foresman, J. B.; Ortiz, J. V.; Cioslowski, J.; Fox, D. J. *Gaussian 09*, Revision D.01; Gaussian, Inc: Wallingford, CT, 2013.

https://doi.org/10.1021/acs.inorgchem.1c00737
Inorg. Chem. 2021, 60, 8790−8801

(88) Grimme, S. Semiempirical Hybrid Density Functional with Perturbative Second-Order Correlation. *J. Chem. Phys.* **2006**, *124*, 034108.
(89) Johnson, E. R.; Becke, A. D. A Post-Hartree-Fock Model of Intermolecular Interactions: Inclusion of Higher-Order Corrections. *J. Chem. Phys.* **2006**, *124*, 174104.
(90) Weigend, F.; Ahlrichs, R. Balanced Basis Sets of Split Valence, Triple Zeta Valence and Quadruple Zeta Valence Quality for H to Rn: Design and Assessment of Accuracy. *Phys. Chem. Chem. Phys.* **2005**, *7*, 3297−3305.
(91) Bergner, A.; Dolg, M.; Küchle, W.; Stoll, H.; Preuß, H. Ab Initio Energy-Adjusted Pseudopotentials for Elements of Groups 13−17. *Mol. Phys.* **1993**, *80*, 1431−1441.
(92) Mitoraj, M.; Michalak, A. Natural orbitals for chemical valence as descriptors of chemical bonding in transition metal complexes. *J. Mol. Model.* **2007**, *13*, 347−355.
(93) Neese, F. Software Update: the ORCA Program System, Version 4.0. *Wiley Interdiscip. Rev.: Comput. Mol. Sci.* **2018**, *8*, No. e1327.
(94) Chai, J.-D.; Head-Gordon, M. Systematic Optimization of Long-Range Corrected Hybrid Density Functionals. *J. Chem. Phys.* **2008**, *128*, 084106.
(95) Grimme, S.; Antony, J.; Ehrlich, S.; Krieg, H. A Consistent and Accurate Ab Initio Parametrization of Density Functional Dispersion Correction (DFT-D) for the 94 Elements H-Pu. *J. Chem. Phys.* **2010**, *132*, 154104.
(96) Grimme, S.; Ehrlich, S.; Goerigk, L. Effect of the Damping Function in Dispersion Corrected Density Functional Theory. *J. Comput. Chem.* **2011**, *32*, 1456−1465.
(97) Glendening, J. K.; Badenhoop, A. E.; Reed, J. E.; Carpenter, J. A.; Bohmann, C. M.; Morales, P. K.; Landis, C. R.; Weinhold, F. *NBO 7.0*; Theoretical Chemistry Institute, University of Wisconsin: Madison, WI, 2018.
(98) Frisch, M. J. T. G. W.; Schlegel, H. B.; Scuseria, G. E.; Robb, M. A.; Cheeseman, J. R.; Scalmani, G.; Barone, V.; Petersson, G. A.; Nakatsuji, H.; Li, X.; Caricato, M.; Marenich, A. V.; Bloino, J.; Janesko, B. G.; Gomperts, R.; Mennucci, B.; Hratchian, H. P.; Ortiz, J. V.; Izmaylov, A. F.; Sonnenberg, J. L.; Williams-Young, D.; Ding, F.; Lipparini, F.; Egidi, F.; Goings, J.; Peng, B.; Petrone, A.; Henderson, T.; Ranasinghe, D.; Zakrzewski, V. G.; Gao, J.; Rega, N.; Zheng, G.; Liang, W.; Hada, M.; Ehara, M.; Toyota, K.; Fukuda, R.; Hasegawa, J.; Ishida, M.; Nakajima, T.; Honda, Y.; Kitao, O.; Nakai, H.; Vreven, T.; Throssell, K.; Montgomery, J. A., Jr.; Peralta, J. E.; Ogliaro, F.; Bearpark, M. J.; Heyd, J. J.; Brothers, E. N.; Kudin, K. N.; Staroverov, V. N.; Keith, T. A.; Kobayashi, R.; Normand, J.; Raghavachari, K.; Rendell, A. P.; Burant, J. C.; Iyengar, S. S.; Tomasi, J.; Cossi, M.; Millam, J. M.; Klene, M.; Adamo, C.; Cammi, R.; Ochterski, J. W.; Martin, R. L.; Morokuma, K.; Farkas, O.; Foresman, J. B.; Fox, D. J. *Gaussian 16*, Revision C.01; Gaussian, Inc.: Wallingford, CT, 2016.

https://doi.org/10.1021/acs.inorgchem.1c00737
Inorg. Chem. 2021, 60, 8790−8801